Soft Matter

Accepted Manuscript

This is an *Accepted Manuscript*, which has been through the Royal Society of Chemistry peer review process and has been accepted for publication.

Accepted Manuscripts are published online shortly after acceptance, before technical editing, formatting and proof reading. Using this free service, authors can make their results available to the community, in citable form, before we publish the edited article. We will replace this *Accepted Manuscript* with the edited and formatted *Advance Article* as soon as it is available.

You can find more information about *Accepted Manuscripts* in the Information for Authors.

Please note that technical editing may introduce minor changes to the text and/or graphics, which may alter content. The journal's standard Terms & Conditions and the Ethical guidelines still apply. In no event shall the Royal Society of Chemistry be held responsible for any errors or omissions in this *Accepted Manuscript* or any consequences arising from the use of any information it contains.

ROYAL SOCIETY OF CHEMISTRY

www.rsc.org/softmatter

Journal Name

RSCPublishing

ARTICLE

Self-assembly of Janus Ellipsoids: a Brownian Dynamics Simulation with a Quantitative Nonspherical-Particle Model

Cite this: DOI: 10.1039/x0xx00000x

Received 00th January 2015,
Accepted 00th January 2015

DOI: 10.1039/x0xx00000x

www.rsc.org/

Jing Xu,[a] Yali Wang,[a] Xuehao He[a*]

Janus ellipsoid as a mesoscale building block can aggregate into variously micelle-like structures in solution that have potential applications in many fields such as novel surfactant, photonic crystal, drug delivery and biochemical sensor. In this work, we present a novel nonspherical-particle model to investigate the self-assembly of Janus ellipsoid, which quantitatively reflects interaction dependence on particle shape. The phase diagrams of Janus ellipsoids depending on aspect ratio and component ratio are achieved and various aggregates are observed such as sandwich-type structure, columnar aggregate, vesicle, liquid crystal, random aggregation structure, spherical micelle and wormlike micelle. The specific heat capacity curves and temperature evolutions illustrate the formation processes of assembled superstructures detailedly. We analyze the potential energy surfaces (PESs) of interaction between two Janus ellipsoids and the minimum energy paths (MEPs) between saddle points on the PESs. It is found that the number of metastable conformation and the activation energy along MEPs rely not only on ellipsoidal shape but also on component ratio. This work provides rich and valuable information for deep understanding the self-assembly mechanism of Janus ellipsoids and design of new mesoscale building blocks.

I. Introduction

Janus particles, a type of building blocks with two or more distinct surfaces,[1] have received considerable attention over the past few decades.[2-7] Owing to anisotropic surface properties, Janus particles can self-assemble into a number of fascinating superstructures that cannot be obtained by homogeneous particles.[8-13] These aggregates with desired structures have potential applications in the fields of novel surfactant,[14] photonic crystal,[15] drug delivery[16] and biochemical sensor.[17] The self-assembly processes of spherical Janus particles, both in theory and experiment, have been intensively studied.[18-21] The anisotropic features of spherical Janus particles such as patchy shape, patchy symmetry and patchy surface fraction govern their assemblies into exotic superstructures rather than simple hexagonal or cubic closest packing.[22-26]

The shape anisotropy can provide new opportunity to richen colloidal self-assembly at a higher level of complexity because self-assembled structures of the particles depend not only on the surface interaction but also on the particle orientation induced by shape anisotropy. For example, self-assembly of Janus cylinders can create fibrillar networks with different pore sizes and different surface compositions by changing the concentration and deposition time of particles.[27] Walther *et al.* also studied the colloidal self-assembly of Janus discs and found sandwich-type structures via back-to-back stacking.[28] Specially, Zerrouki *et al.* discovered the chiral colloidal clusters from the assembly of asymmetric dumbbell-shaped magnetic particles in an external magnetic field.[29] It indicates that the shape anisotropy is an effective method to tune the morphologies of aggregates. The systematical study about the dependence of shape and surface interaction of Janus particle is necessary.

Janus ellipsoid is a typical Janus particle with anisotropic shape to investigate the relationship between building block shape and morphology of superstructure. In experiments, Janus ellipsoids have been successfully synthesized and the self-assemblies of Janus ellipsoids with different shapes were studied in the past.[30-37] Distinctive aggregations including one-dimension fibres and two-layer face-to-face stacks were observed, whose morphologies could be tuned by changing aspect ratio. Inspired by Kern-Frenkel model,[38] Gunton and coworkers proposed a simple Janus ellipsoid model with a quasi-square-well potential which is modified by an orientational factor and studied the effects of the aspect ratio of ellipsoid on the self-assembly.[39-42] However, their model is only suitable for Monte Carlo simulation because of the inconsecutive potential and the accurate dynamics of the system is unavailable. To fully understand the effect of the particle orientation induced by shape anisotropy on dynamic process, a better prediction of interaction between ellipsoidal nanoparticles calls for detailed investigation.

In this report, we introduce a novel nonspherical-particle model to study the self-assembly of Janus ellipsoids where the potential between particles is described as an orientation-dependent coarse-grained formula, and the parameters in our model are extracted from the all-atom objects. The method not only quantitatively reflects interaction with different particle orientation but also provides high computation efficiency in simulation. The sensitivities of self-assembled structure of Janus ellipsoid to the aspect ratio and component ratio are systematically studied with Brownian Dynamics method. The Janus particle is constructed with two different subunits

Soft Matter Accepted Manuscript

(coarse-grained beads or atoms) on two hemi-surfaces of ellipsoid. Very rich hierarchical structures are observed including sandwich-type structure, columnar aggregate, vesicle, liquid crystal, random aggregation structure, spherical micelle and wormlike micelle, and the phase diagrams of Janus ellipsoids are presented. Further, the transition path of two metastable conformations is analyzed using the minimum energy paths (MEPs) method according the potential energy surfaces (PESs) between two Janus ellipsoids. In section II, Janus ellipsoid model is described in detail and the interaction between Janus particle as well as Brownian Dynamics simulation algorithm is interpreted. The simulation results and discussions are presented in section III and the simulation conclusion is shown in section IV.

II. Model and Algorithm

In our simulation, hollow Janus ellipsoid is constructed by two types of coarse-grain beads, denoted by A (blue) and B (green), respectively, and the beads are almost homogeneously distributed on the ellipsoid surface with equal arc length in both longitude and latitude. For changing the aspect ratio, which denotes the ratio of the minor axis to the major axis ($\lambda = b/a$), the length of major axis a is fixed at 3.0 nm and the length of the minor axis b varies. By changing the length of the minor axis b, the shapes of Janus ellipsoids change from oblate, via spherical, to prolate form (Fig.1a). The component ratio of Janus particles is defined as $x = N_A / N_{total}$ where N_A is the number of A bead and N_{total} is the number of total beads as shown in Fig.1b.

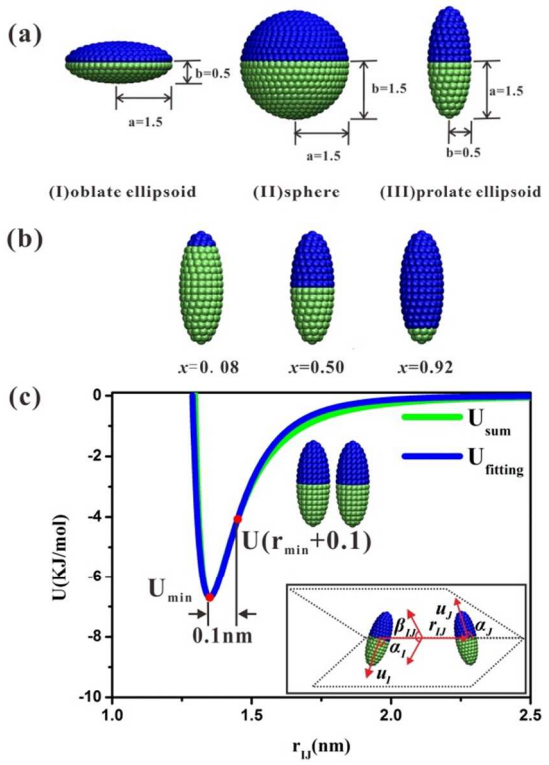

Fig.1 (a) Representatives of Janus ellipsoids. Particle I is an oblate ellipsoid with $\lambda_o = 0.33$, particle II is a sphere with $\lambda = 1.00$ and particle III is a prolate ellipsoid with $\lambda_p = 0.33$. (b) Janus ellipsoids with different component ratio ($\lambda_p = 0.33$). (c) The energy curves obtained by summation and fitting methods of prolate Janus ellipsoid ($\lambda_p = 0.33$, $x = 0.50$) with $\alpha_I = 0.5\pi$, $\alpha_J = 0.5\pi$, $\beta_{IJ} = 0.0$. $\boldsymbol{r}_{IJ} = \boldsymbol{r}_I - \boldsymbol{r}_J$ is the inter-particle vector of particle I, J. $\boldsymbol{u}_I$, $\boldsymbol{u}_J$ is the orientation vector of particle I, J. α_I represents the angle between $\boldsymbol{u}_I$ and $\boldsymbol{r}_{IJ}$, α_J represent the angle between $\boldsymbol{u}_J$ and $\boldsymbol{r}_{IJ}$, β_{IJ} represent the dihedral angle between $\boldsymbol{u}_I$ and $\boldsymbol{u}_J$.

The coarse-grained beads in two Janus ellipsoids interact with each other through Lennard-Jones potential $U_0 = 4\varepsilon_{ij}((\sigma_{ij}/r_{ij})^{12} - (\sigma_{ij}/r_{ij})^6)$ where ε_{ij} is the depth of potential well, σ_{ij} is the finite distance at which the inter-particle potential is zero, r_{ij} is the distance between the particles. And $\varepsilon_{AA} = 0.04$ kJ/mol, $\varepsilon_{BB} = 0.006$ kJ/mol, $\varepsilon_{AB} = 0.004$ kJ/mol and $\sigma_{AA} = \sigma_{BB} = \sigma_{AB} = 0.04$ nm are employed. As a result, the interaction between two Janus ellipsoids (denoted by I and J particles) equals the sum of potential of coarse-grain beads, which can be expressed as

$$U_{IJ} = \sum_{i\in I}\sum_{j\in J} U_0 \quad (1).$$

In principle, the dissipative force and charge interaction can be introduced into the coarse-grained units or beads in mapping process. It will be considered in future work. In our system, Janus ellipsoids are regarded as rigid bodies. When Janus particles move or rotate, the interaction potential between two Janus particles should be newly calculated from the interaction sum between all coarse-grain beads in Janus ellipsoids in every time step. It results in very large cost of computation time especially when the constructed bead in a particle is up to hundred or thousand. To improve the simulation efficiency, the coarse-grain potential U_{IJ} between two Janus ellipsoids is proposed using fitting method and tabulated technology. The anisotropic coarse-grain potential U_{IJ} can be written as

$$U_{IJ} = 4\varepsilon_e\left[\left(\frac{\sigma_e}{r_{IJ}-\Delta r_e}\right)^{12} - \left(\frac{\sigma_e}{r_{IJ}-\Delta r_e}\right)^{6}\right] \quad (2)$$

Here, strength parameter ε_e, shape parameter Δr_e and range parameter σ_e are all orientation dependent, and the orientation is described as α_I, α_J, β_{IJ}. As the inset in Fig.1c shows, α_I is the orientation angle of particle I, α_J is the orientation angle of particle J, β_{IJ} is the dihedral angle between particle I and particle J, and r_{IJ} is the center-to-center distance of two particles. The ranges of these orientation angle are set as $\alpha_I \in [0,\pi]$, $\alpha_J \in [0,\pi]$ and $\beta_{IJ} \in [0,\pi]$.

The interaction potential of two ellipsoid particles is a function of orientation parameters α_I, α_J, β_{IJ}, and distance r_{IJ}. Fig.1 only shows the potential curve for a set of orientation parameters ($\alpha_I = 0.5\pi$, $\alpha_J = 0.5\pi$, $\beta_{IJ} = 0.0$). The potential profiles depending on β_{IJ} at fixed α_I and α_J are provided in Fig.S3. For different orientation parameters, the potential curves are similar and the major differences are the lowest value of the potential energy, the shape and position of the potential curve. These values of ε_e, σ_e and Δr_e are achieved by fitting eq.1 to eq.2. The target potential curve of U_{IJ} is firstly calculated using eq.1 and then the values of ε_e, σ_e, Δr_e are solved in term of two potentials at r_{min} and $r_{min} + 0.1$ where r_{min} is the particle distance for lowest potential energy U_{min}. As shown in Fig.1c, the fitting curve well exhibits properties of the target curve in the major attractive zone.

To directly perceive the relationship of potential energy and orientation of two Janus ellipsoids, one hundred discrete points are interpolated into the limited range of each orientation angle (i.e., α_I, α_J, β_{IJ}) to construct the tabulated potential between two ellipsoids. According to the tabulated potential, the interaction energy of two Janus particles with an arbitrary orientation can be calculated with the interpolation technology.[43] After achieving the potential of Janus particles, the rigid body Brownian Dynamics simulation is carried out. The conformation space trajectories are composed of successive displacement and rotation in each time step Δt. The displacement and rotation motions satisfy the following equations

Soft Matter Accepted Manuscript

$$\boldsymbol{r}(t+\Delta t)=\boldsymbol{r}(t)+\Delta t\frac{\xi_t}{m}\boldsymbol{F}+\sqrt{\frac{6k_BT\Delta t\xi_t}{m}}\cdot\boldsymbol{\zeta} \quad (3)$$

$$\boldsymbol{Q}(t+\Delta t)=\boldsymbol{Q}(t)+\Delta t\frac{\boldsymbol{Q}\xi_r\boldsymbol{\tau}}{2m_I}+\boldsymbol{Q}\sqrt{\frac{3k_BT\Delta t\xi_r}{2m_I}}\cdot\boldsymbol{\zeta} \quad (4)$$

Where the position of the Janus particle is represented by $\boldsymbol{r}$ and the rotation of the Janus particle is described by quaternion $\boldsymbol{Q}$. ξ_t and ξ_r denote friction constants in translation motion and rotation motion respectively. k_B is Boltzmann constant and $\boldsymbol{\zeta}$ is standard Gaussian distributed noise. $\boldsymbol{\tau}$ is torque in rotation and $\boldsymbol{F}$ is translation force. They can be numerically calculated with the formulas $\tau=-(E_{\theta+d\theta}-E_{\theta-d\theta})/2d\theta$, $F=-(E_{r+dr}-E_{r-dr})/2dr$, where E_{r+dr}, E_{r-dr}, $E_{\theta+d\theta}$, $E_{\theta-d\theta}$ are potential energies obtained by Catmull-Rom interpolation method[43] from tabulated potential energy. Here, r is particle position and θ is particle orientation angle. For the precision of calculation, very small $d\theta$ =1.0×10^{-5} rad and dr =1.0×10^{-5} nm are used. m and m_I are the moment of inertia and the mass of particles (m =1.33 u and m_I =1.02 $u\cdot\mathrm{nm}^2\cdot\mathrm{rad}^{-2}$). The cut off distance r_c = 8.0 nm is much larger than Janus particle size. To further improve the simulation efficiency and quicken convergence of the system, the soft-core potential is introduced when r_{IJ} is less than r_{min} (r_{min} is the distance at which the potential reaches its minimum, r_{min} = Δr_e+2$^{1/6}\sigma_e$, according to eq. 2). Thus, the final form of the anisotropic potential is described as follows

$$U_{IJ}=\begin{cases}0.5(U_{\max}+\varepsilon_e)\cos(\frac{r_{IJ}}{r_m}\pi)+0.5(U_{\max}-\varepsilon_e) & r_{IJ}<r_{min}\\ 4\varepsilon_e\left[\left(\frac{\sigma_e}{r_{IJ}-\Delta r_e}\right)^{12}-\left(\frac{\sigma_e}{r_{IJ}-\Delta r_e}\right)^{6}\right] & r_{min}\le r_{IJ}\le r_c\\ 0 & r_{IJ}>r_c\end{cases} \quad (5)$$

According to simulation experience, U_{max} is set as U_{max} = 500 kJ/mol and U_{IJ} is equal to U_{max} at r_{IJ} = 0.

The hydrodynamic interactions is not considered due to no explicit solvent molecules. Our model is suitable to study thermodynamic properties of self-assembly of nonspherical particles. The simulations are carried out in a cubic box (18×18×18 nm^3) with periodic boundary conditions using 50 particles which are randomly distributed with random orientations at initial state. We also examined the simulation using more particles (200 particles in a cubic box of 28.6×28.6×28.6 nm^3, see Figures S4 and S5). There is no obvious difference with the results of 50 particles. For computation time, 50 particles are mainly used in the simulations to explore phase diagram. In simulation process, an annealing operation with 20000 steps/K is used to achieve equilibrium aggregation structure. The friction constants in translation motion and rotation motion are ξ_t = 0.005 ps^{-1} and ξ_t = 0.005 ps^{-1}, and the integration time step Δt =0.02 ps is employed. In order to compare the influences of ellipsoidal shape and component ratio on the aggregation temperature, the reduced temperature is usedd in the simulations which is defined as $T^*=k_BT/\varepsilon_{min}$ and the corresponding reduced potential energy is expressed as $E^*=E/\varepsilon_{min}$, where ε_{min} is the well depth of the potential energy of two ellipsoids with the single A component at the optimal conformation.

III. Results and Discussion

In our simulations, annealing operations are carried out from high temperature (corresponding to a dispersed state) to aggregation temperature in order to achieve final equilibrium structures. Upon varying the aspect ratio λ and component ratio x, the phase diagrams of Janus oblate and prolate ellipsoids are obtained at a specific aggregation temperature T^* = 0.374, as shown in Fig.2 and Fig.3. Typical assembled structures are also presented in Fig.2 and Fig.3. For oblate Janus ellipsoid (Fig.2), the phase diagram is divided into eight regions: monomers (region I), columnar aggregate (region II), dimers (region III), vesicle (region IV), random aggregation structure (region V), lamellae (region VI), wormlike micelle (region VII) and spherical micelles (region VIII). The aggregation process of Janus particles is similar to the "particle polymerization" and the Janus particles can be regarded as monomers in the polymerization. In region I, no obvious aggregate is obtained and ellipsoids are distributed randomly (Fig.2a). With increasing x, oligomers appear in region III and VIII. Janus ellipsoids self-assemble into sandwich-like dimers (Fig.2c) when the blue faces of two ellipsoids contact with each other at small λ_o and spherical micelles (Fig.2h) are observed at big λ_o. The larger x is the stronger attraction between two ellipsoids is. With further increasing x, we obtain lamellae (Fig.2f) in region VI, wormlike structure (Fig.2g) in region VII and even vesicle (Fig.2d) in region IV. When x is very large (region II and region V), the interaction between Janus ellipsoids is strengthened because of the large fraction of strong attractive patch, and it is probably to observe random aggregation structure (Fig.2e) except that columnar aggregate (Fig.2b) appears at very small λ_o owing to the unique oblate shape.

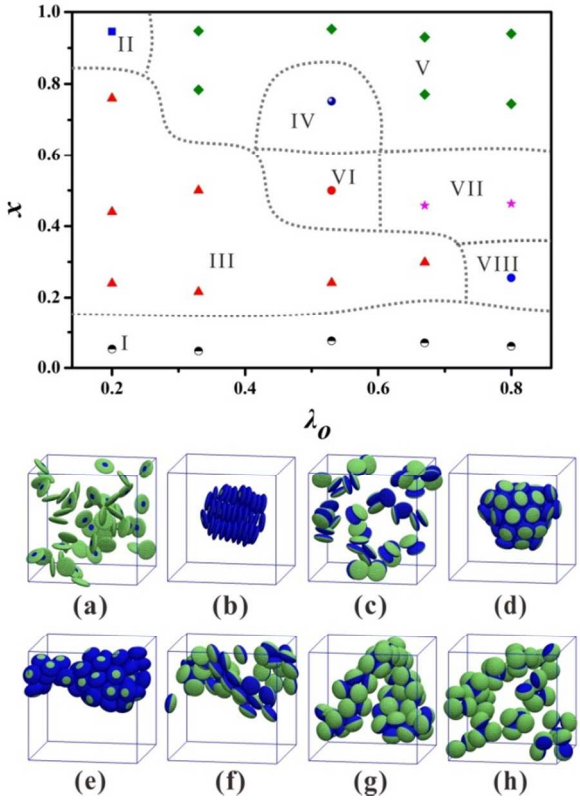

Fig.2 Phase diagram of oblate Janus ellipsoid in λ_o - x plane. Typical equilibrium self-assembled structures are shown: (a) monomers of oblate Janus ellipsoid in region I (λ_o = 0.20, x = 0.05). (b) columnar aggregate in region II (λ_o = 0.20, x = 0.95). (c) sandwich-like dimers in region III (λ_o = 0.33, x = 0.50). (d) vesicle in region IV (λ_o = 0.53, x = 0.75). (e) random aggregation structure in region V (λ_o = 0.67, x = 0.92). (f) lamellae in region VI (λ_o = 0.53, x = 0.50). (g) wormlike structure in region VII (λ_o = 0.80, x = 0.47). (h) spherical micelles in region VIII (λ_o = 0.80, x = 0.26).

Soft Matter Accepted Manuscript

When the shape of Janus ellipsoid changes from oblate ellipsoid, via sphere, to prolate ellipsoid, the phase structures are also various which depend on the aspect ratio and component ratio. The phase diagram of prolate Janus ellipsoid can be divided into six regions: monomers (region I), liquid crystal (region II), spherical micelles (region III), wormlike micelle (region IV), random aggregation structure (region V) and dimers (region VI). In region I, Janus ellipsoids distributed as monomers (Fig.3a) due to weaker interaction. When the shapes of ellipsoids are close to or equal to sphere with a weak interaction, particles tend to form dimers (as shown in Fig.3f in region VI.). Liquid crystal (Fig.3b) appears in region II because this ordered structure can guarantee the maximum contact surface of strong attractive patch with large x and small λ_p. Spherical and wormlike micelle form in region III and IV, and the formations of these structures are similar to the micellization of surfactant molecules, a structure with a hydrophilic outer layer and a hydrophobic core. Further increasing λ_p, ellipsoids aggregate into a large random aggregation structure (as shown in Fig.3e in region V), like the structure in Fig.2e. In addition, the phase diagrams of final aggregates whose morphologies do not change dramatically with temperature further decreasing are shown in Fig.S1 and Fig.S2. At very low temperature, all particles in the system assemble into one big aggregate at full range of component ratio and aspect ratio. For oblate ellipsoid, monomers and dimers in Fig.2 further assemble into columnar aggregate, lamella or random aggregation structure. Moreover, spherical micelles in Fig.2 interact with each other and translate to wormlike structure finally. For prolate ellipsoid, monomers and dimers in Fig.3 also attract each other forming liquid crystal, spherical micelles or random aggregation structure.

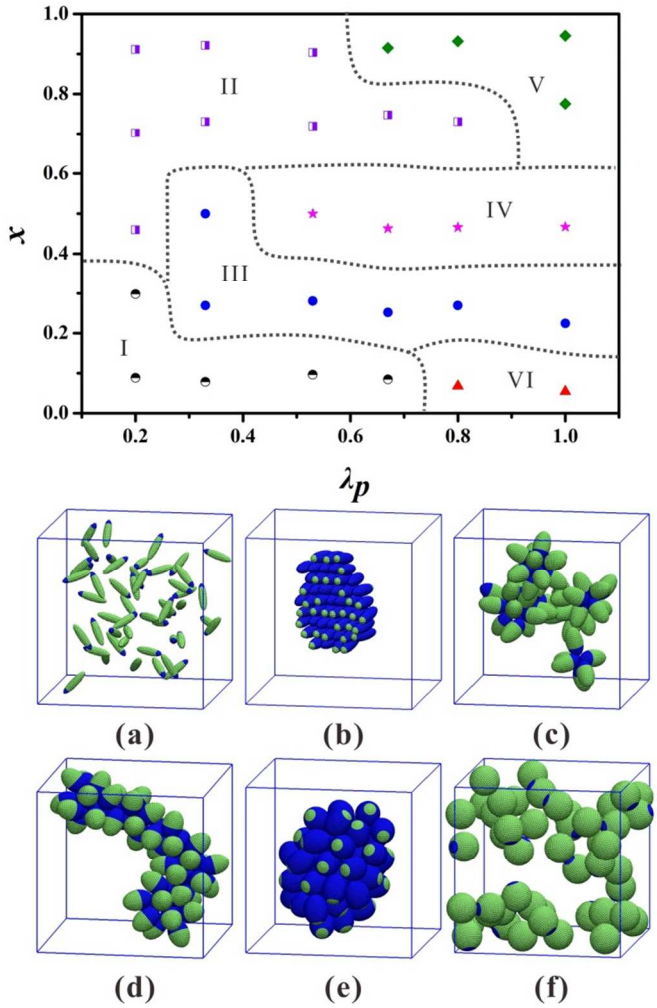

Fig.3 Phase diagram of prolate Janus ellipsoid in the $\lambda_p - x$ plane. Typical equilibrium self-assembled structures of each region are shown: (a) monomers of prolate Janus ellipsoid in region I (λ_p = 0.20, x = 0.09). (b) liquid crystal in region II (λ_p = 0.33, x = 0.92). (c) spherical micelles in region III (λ_p = 0.53, x = 0.28). (d) wormlike micelle in region IV (λ_p = 0.67, x = 0.46). (e) random aggregation structure in region V (λ_p = 0.80, x = 0.91). (f) dimers of prolate Janus ellipsoid in region VI (λ_p = 1.00, x = 0.05).

The aspect ratio and component ratio collaborate to govern the assembled structures of Janus oblate and prolate ellipsoids as shown in Fig.2 and Fig.3, but increasing λ and x has different influences on the self-assembled structures. Increasing λ represents a smaller deformability of Janus ellipsoid and its phase behavior is similar to that of Janus sphere. In fact, increasing x means broadening the range of strong interaction. At smaller x, the interaction between Janus ellipsoids is weak, and ellipsoids are hard to form large aggregates. At relatively larger x, the interaction between Janus ellipsoids is enough strong to assemble into large ordered clusters with specific morphology.

To understand general thermodynamics of Janus ellipsoid, the specific heat capacity C_v in the process of annealing is calculated. It is derived from potential energy, that is,

$$Cv = \frac{\partial \langle E \rangle}{\partial T} = \frac{1}{k_B T^2}\left(\langle E^2 \rangle - \langle E \rangle^2\right) = \frac{k_B}{(T^*)^2}\left(\langle (E^*)^2 \rangle - \langle E^* \rangle^2\right) \quad (6)$$

Fig.4a shows specific heat capacity curves of four representative superstructures of oblate ellipsoids. We can observe a pronounced maximum on each curve, indicating that there is an abrupt change of potential energy in this narrow temperature range, and the corresponding temperature with maximal C_v is defined as transition temperature T_a^*. Then, we check the dynamic evolutions of ellipsoids from high temperature via T_a^* to T^* = 0.374. At initial high temperatures, i.e. the top row of Fig.5a-d, Janus ellipsoids are randomly distributed in the simulation boxes, and then these disordered free Janus ellipsoids transform into directional oligomers when annealing temperatures decrease from initial temperatures to T_a^*. These oligomers then adjust their orientations to guarantee the biggest contact surface of strong attractive patch of ellipsoids with the annealing temperature decrease. And interesting structures including columnar aggregate, vesicle, random aggregation structure and wormlike micelle appears at T^* = 0.374.

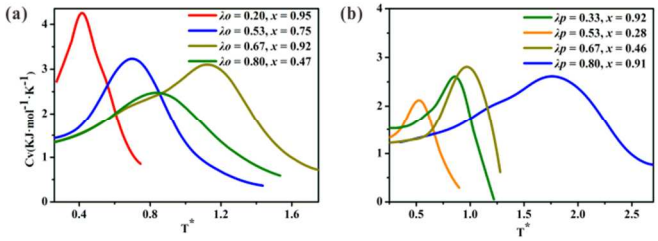

Fig.4 (a) Specific heat capacity curves of four representative superstructures of oblate ellipsoids (b) Specific heat capacity curves of four representative superstructures of prolate ellipsoids.

Soft Matter Accepted Manuscript

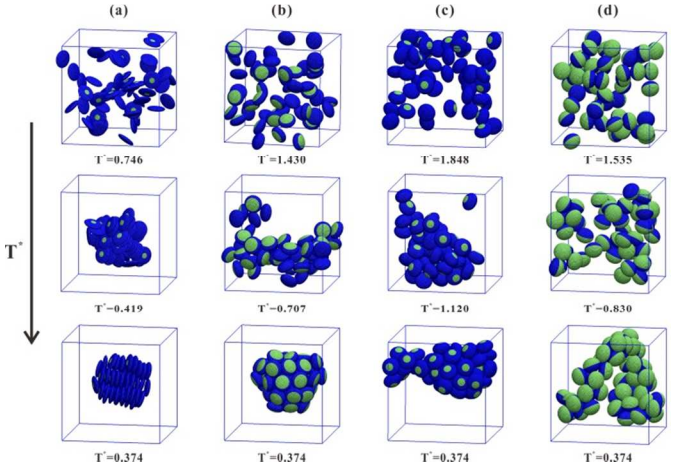

Fig.5 Representative evolution snapshots of four representative superstructures of oblate ellipsoids: (a) columnar aggregate at λ_o = 0.20, x = 0.95, (b) vesicle at λ_o = 0.53, x = 0.75, (c) random aggregation structure at λ_o = 0.67, x = 0.92, (d) wormlike micelle at λ_o = 0.80, x = 0.47.

For prolate Janus ellipsoid, the C_v curves (Fig.4b) and conformation temperature evolutions (Fig.6) of superstructures are different to that of oblate ellipsoid. Just as oblate Janus ellipsoid, prolate Janus ellipsoids are disordered monomers at high temperature (Fig.6a-d). These monomers interact with different orientations forming oligomers in the process of temperature decreasing to T_a^* . The oligomers further attract each other and ultimately coalesce to form big aggregate with temperature further decreasing, and structures including liquid crystal, spherical micelle, wormlike micelle and random aggregation structure form through the growth and rearrangement process.

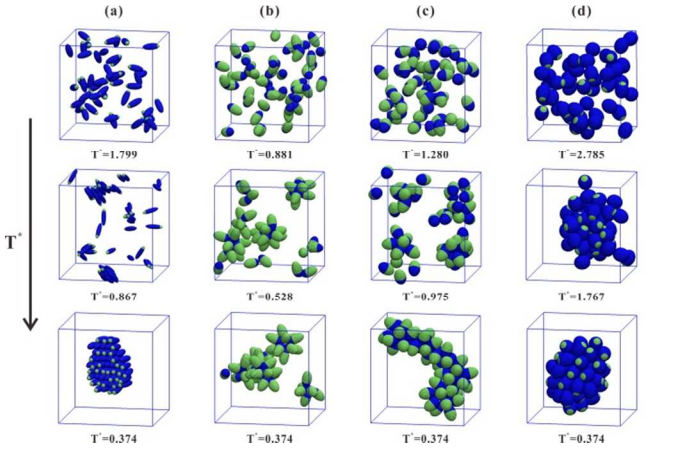

Fig.6 Representative evolution snapshots of four representative structures of prolate ellipsoids: (a) liquid crystal at λ_p = 0.33, x = 0.92, (b) spherical micelle at λ_p = 0.53, x = 0.28, (c) wormlike micelle at λ_p = 0.67, x = 0.46, (d) random aggregation structure at λ_p = 0.80, x = 0.91.

To deeply explore formation mechanisms of the self-assembled structures of Janus ellipsoids, we search the potential energy surfaces (PESs) between two ellipsoids and confirm the metastable and stable conformations with random searching implies that transition between conformation 3 and 1 becomes method (Fig.7 and Fig.8). Finally, the minimum energy paths (MEPs) among these configurations are calculated using the improved string method[44] The metastable and stable conformations for oblate Janus ellipsoids with different λ and x are shown in Fig.7a-c and the energy curves along the MEPs as well as corresponding activation energies (E_a) between saddle points are shown in Fig.7d-f. The PES shapes and the conformations of metastable and stable states are similar, but the transition activation energies are quite different. As x increases (Fig.7d and Fig.7e), the transition activation energy between conformation 3 and 1 decreases obviously because the increment of fraction of strong interaction patch induces the Janus ellipsoids to stack with blue-to-blue conformation, which implies that transition between conformation 3 and 1 becomes more easily. Specially, all transition activation energies decrease with increasing λ (Fig.7f and Fig.7e). Since the aspect ratio λ increases, the shape of oblate ellipsoid is closer to sphere, leading to smaller contact surface between two ellipsoids and weakening the strength of interaction.

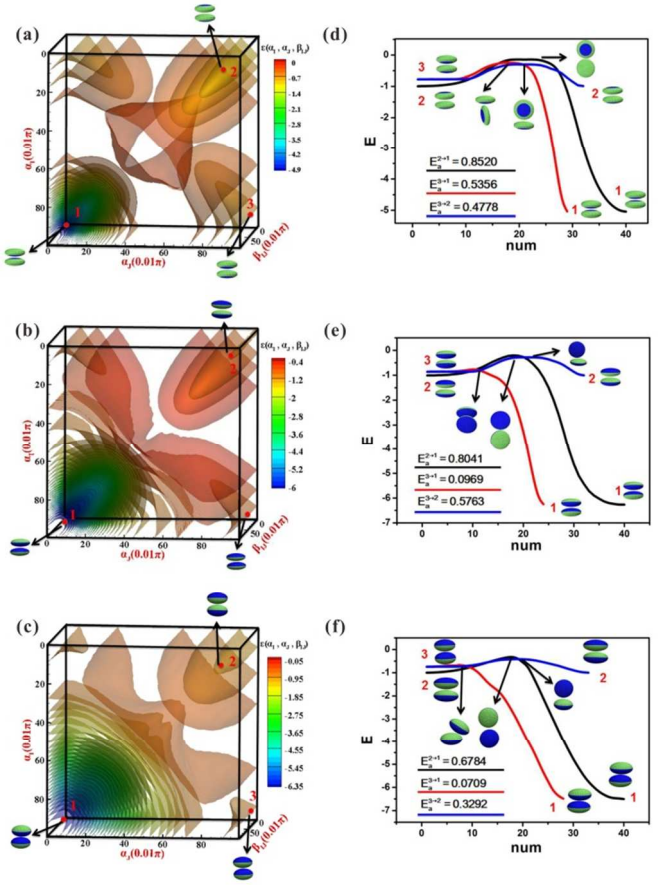

Fig.7. Three-dimensional isosurface plots of potential energy and energy curves along the MEPs between saddle points of oblate Janus ellipsoids at λ_o = 0.33, x = 0.22 (a, d); λ_o = 0.33, x = 0.50 (b, e); λ_o = 0.53, x = 0.50 (c, f). The saddle points are marked by red symbols. There are four zones of minima on these PESs, and only three minima are displayed because of symmetry.

For prolate Janus ellipsoid, the effects of λ and x on PESs are quite another thing. There are three minima on PESs when component ratio of prolate ellipsoid is small (Fig.8a), however, as component ratio increases, the number of minima on PESs decreases to two (Fig.8b) and the corresponding activation energy between saddle point 1 and 2 increases (Fig.8d and Fig.8e). When Janus ellipsoid becomes less prolate with λ_p increasing, the location of minima on the PESs is similar (Fig.8b and 8c), but the corresponding transition activation energy decreases obviously (Fig.8e and Fig.8f). The results

Soft Matter Accepted Manuscript

reveal that aspect ratio λ and component ratio x have great effects on the self-assembly of Janus ellipsoid. Aspect ratio λ mainly affects the contact surface between particles while the component ratio x mostly determine the strength of interaction between particles.

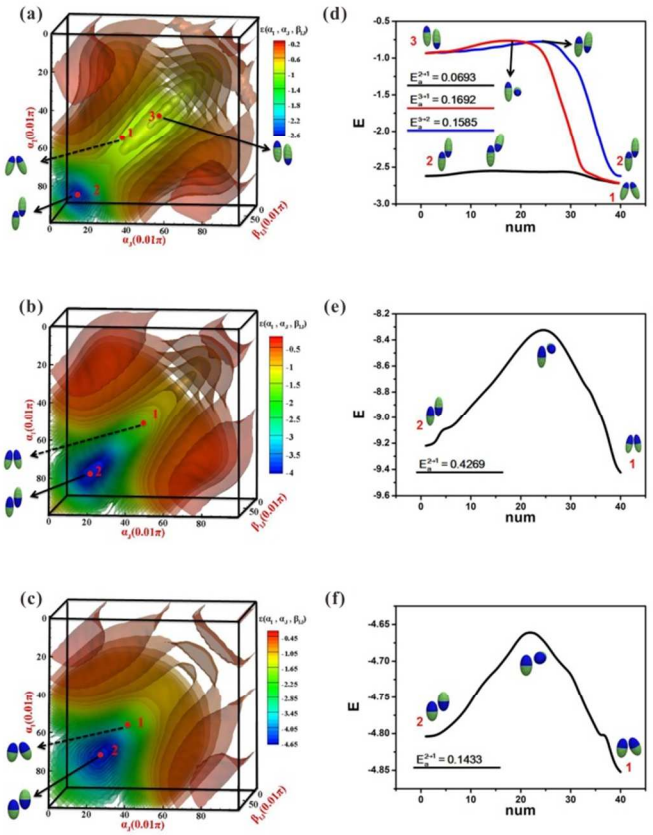

Fig.8. Three-dimensional isosurface plots of potential energy and energy curves along the MEPs between saddle points of prolate Janus ellipsoids at λ_p = 0.33, x = 0.27 (a, d); λ_p = 0.33, x = 0.50 (b, e); λ_p = 0.53, x = 0.50 (c, f). The saddle points are marked by red symbols.

IV. Conclusions

In summary, we propose a novel nonspherical-particle model to study the self-assembly of Janus ellipsoids including oblate Janus ellipsoid, Janus sphere, and prolate Janus ellipsoid with different aspect ratios and component ratios. In Brownian Dynamics simulations, a combination of the aspect ratio and component ratio generates a number of fascinating structures such as columnar aggregate, vesicle, liquid crystal, spherical micelle and wormlike micelle. The phase diagrams of oblate Janus ellipsoid and prolate Janus ellipsoid are provided, which is of great value for design of building blocks of self-assembly. Moreover, we analyze the specific heat capacity curves and temperature evolutions of the assembled superstructures. The results show that the formation processes are growth and rearrangement processes. Finally, we introduce the PESs and MEPs to understand the formation mechanisms of those fascinating assembled structures further, considering the influences of aspect ratio and component ratio of Janus ellipsoid. Interestingly, the influences on oblate and prolate Janus ellipsoids are quite different; for oblate ellipsoid, the stable configuration is a blue face-to-blue face stacking and the aspect ratio affects the contact surface while the component ratio affects interaction strength. However, for prolate ellipsoid, the component ratio has great influence on the number of metastable conformation on PESs and the aspect ratio determines the activation energy along MEPs. Our results demonstrate that changing structures of building blocks, i.e., the ellipsoidal shape and component ratio, can effectively tune the self-assembly behaviors.

Acknowledgements

The project is supported by the National Natural Science Foundation of China (No. 21474075, 91127046 and 21274107).

Notes and references

[a] Department of Chemistry, School of Science, Tianjin University, (Tianjin), 300072 Tianjin, China.
* Corresponding author, E-mail address: xhhe@tju.edu.cn.

† Electronic Supplementary Information (ESI) available: the phase diagrams of final aggregates whose morphologies do not change dramatically with temperature further decreasing, the potential profiles depending on dihedral angle β_{IJ} and distance r_{IJ}, typical self-assembled structures in larger system. See DOI: 10.1039/b000000x/

1 P.-G. de Gennes, *Angew. Chem. Int. Ed. Engl.,* 1992, **31**, 842.
2 R. Erhardt, A. Böker, H. Zettl, H. Kaya, W. Pyckhout-Hintzen, G. Krausch, V. Abetz and A. H. E. Müller, *Macromolecules,* 2001, **34**, 1069.
3 B. Li, Y.-L. Zhu, H. Liu and Z.-Y. Lu, *Phys. Chem. Chem. Phys.,* 2012, **14**, 4964.
4 Y. Liu, C. Yu, H. Jin, B. Jiang, X. Zhu, Y. Zhou, Z. Lu and D. Yan, *J. Am. Chem. Soc.,* 2013, **135**, 4765.
5 A. Kumar, B. J. Park, F. Tu and D. Lee, *Soft Matter,* 2013, **9**, 6604.
6 T. S. Skelhon, Y. Chen and S. A. F. Bon, *Soft Matter,* 2014, **10**, 7730.
7 J. Hu, S. Zhou, Y. Sun, X. Fang and L. Wu, *Chem. Soc. Rev.,* 2012, **41**, 4356.
8 A. Walther and A. H. E. Müller, *Chem. Rev.,* 2013, **113**, 5194.
9 S. Jiang, Q. Chen, M. Tripathy, E. Luijten, K. S. Schweizer and S. Granick, *Adv. Mater.,* 2010, **22**, 1060.
10 Z.-W. Li, Z.-Y. Lu and Z.-Y. Sun, *Soft Matter,* 2014, **10**, 5472.
11 Z.-W. Li, Z.-Y. Lu, Z.-Y. Sun and L.-J. An, *Soft Matter,* 2012, **8**, 6693.
12 W. Cao, R. Huang, W. Qi, R. Su and Z. He, *ACS Appl. Mater. Interfaces,* 2015, **7**, 465.
13 R. Erhardt, M. Zhang, A. Böker, H. Zettl, C. Abetz, P. Frederik, G. Krausch, V. Abetz and A. H. E. Müller, *J. Am. Chem. Soc.,* 2003, **125**, 3260.
14 Y. K. Takahara, S. Ikeda, S. Ishino, K. Tachi, K. Ikeue, T. Sakata, T. Hasegawa, H. Mori, M. Matsumura and B. Ohtani, *J. Am. Chem. Soc.,* 2005, **127**, 6271.
15 I. D. Hosein, M. Ghebrebrhan, J. D. Joannopoulos and C. M. Liddell, *Langmuir,* 2010, **26**, 2151.
16 X. Xi, J. Wang, X. Dong, Q. Ma, W. Yu and G. Liu, *Chem. Eng. J.,* 2014, **254**, 259.
17 L. K. Bogart, G. Pourroy, C. J. Murphy, V. Puntes, T. Pellegrino, D. Rosenblum, D. Peer and R. Lévy, *ACS Nano,* 2014, **8**, 3107.
18 F. Sciortino, A. Giacometti and G. Pastore, *Phys. Rev. Lett.,* 2009, **103**, 237801.
19 L. Hong, A. Cacciuto, E. Luijten and S. Granick, *Langmuir,* 2008, **24**, 621.
20 T. Vissers, Z. Preisler, F. Smallenburg, M. Dijkstra and F. Sciortino, *J. Chem. Phys.,* 2013, **138**, 164505.
21 F. Romano and F. Sciortino, *Nature Communications,* 2012, **3**.
22 Q. Chen, E. Diesel, J. K. Whitmer, S. C. Bae, E. Luijten and S. Granick, *J. Am. Chem. Soc.,* 2011, **133**, 7725.
23 Q. Chen, S. C. Bae and S. Granick, *Nature,* 2011, **469**, 381.
24 L. Hong, A. Cacciuto, E. Luijten and S. Granick, *Nano Lett.,* 2006, **6**, 2510.
25 G. Munao, Z. Preisler, T. Vissers, F. Smallenburg and F. Sciortino, *Soft Matter,* 2013, **9**, 2652.

Soft Matter Accepted Manuscript

26 Z. Preisler, T. Vissers, G. Munao, F. Smallenburg and F. Sciortino, *Soft Matter,* 2014, **10**, 5121.
27 A. Walther, M. Drechsler, S. Rosenfeldt, L. Harnau, M. Ballauff, V. Abetz and A. H. E. Müller, *J. Am. Chem. Soc.,* 2009, **131**, 4720.
28 A. Walther, X. André, M. Drechsler, V. Abetz and A. H. E. Müller, *J. Am. Chem. Soc.,* 2007, **129**, 6187.
29 D. Zerrouki, J. Baudry, D. Pine, P. Chaikin and J. Bibette, *Nature,* 2008, **455**, 380.
30 J. Liu, G. Liu, M. Zhang, P. Sun and H. Zhao, *Macromolecules,* 2013, **46**, 5974.
31 A. A. Shah, B. Schultz, W. Zhang, S. C. Glotzer and M. J. Solomon, *Nat. Mater.,* 2015, **14**, 117.
32 A. A. Shah, B. Schultz, K. L. Kohlstedt, S. C. Glotzer and M. J. Solomon, *Langmuir,* 2013, **29**, 4688.
33 J. Yan, K. Chaudhary, S. C. Bae, J. A. Lewis and S. Granick, *Nature Communications,* 2013, **4**.
34 P. Tierno, R. Albalat and F. Sagues, *Small,* 2010, **6**, 1749.
35 T. Deng, J. R. Cournoyer, J. H. Schermerhorn, J. Balch, Y. Du and M. L. Blohm, *J. Am. Chem. Soc.,* 2008, **130**, 14396.
36 S. Shen, T. Gu, D. Mao, X. Xiao, P. Yuan, M. Yu, L. Xia, Q. Ji, L. Meng, W. Song, C. Yu and G. Lu, *Chem. Mater.,* 2012, **24**, 230.
37 O. Guell, F. Sagues and P. Tierno, *Adv. Mater.,* 2011, **23**, 3674.
38 N. Kern and D. Frenkel, *J. Chem. Phys.,* 2003, **118**, 9882.
39 Y. Liu, W. Li, T. Perez, J. D. Gunton and G. Brett, *Langmuir,* 2012, **28**, 3.
40 W. Li and J. D. Gunton, *Langmuir,* 2013, **29**, 8517.
41 D. P. Ruth, J. D. Gunton, J. M. Rickman and W. Li, *J. Chem. Phys.,* 2014, **141**, 214903.
42 W. Li, Y. Liu, G. Brett and J. D. Gunton, *Soft Matter,* 2012, **8**, 6027.
43 E. Catmull and R. Rom In *Computer Aided Geometric Design*; Riesenfeld, R. E. B. F., Ed.; Academic Press: 1974, p 317.
44 W. E, W. Ren and E. Vanden-Eijnden, *J. Chem. Phys.,* 2007, **126**, 164103.

Soft Matter Accepted Manuscript